Received: 29 June 2024 | Revised: 7 October 2024 | Accepted: 7 October 2024

IET Radar, Sonar & Navigation

DOI: 10.1049/rsn2.12654

The Institution of Engineering and Technology WILEY

ORIGINAL RESEARCH

# Measurements and analysis of the radar cross section of chaff dipoles

**Alessio Balleri**[1] | **Brian Butters**[2]

[1]Centre for Electronic Warfare, Information and Cyber, Cranfield University, Defence Academy of the UK, Shrivenham, UK

[2]Meon Technology Ltd, Emsworth, UK

**Correspondence**

Alessio Balleri.
Email: a.balleri@cranfield.ac.uk

**Funding information**

Defence Science and Technology Laboratory, Grant/Award Number: DSTL/AGR/00623/01

## Abstract

A free space test method to measure the Radar Cross Section (RCS) of single dipole elements is presented. The method is such that dipoles can be measured over a large range of frequencies, in free space and without the need of an anechoic chamber. The setup employs with a Vector Network Analyser (VNA) synchronised to a rotating turntable that controls the position of the transmitting and receiving antennas and the polarisation of the irradiated electric field. Measurements are collected for chaff dipoles made of copper wire, microwire and aluminised glass, from 5 to 11 GHz, to allow a comparison of chaff RCS properties with respect to chaff material and method of fabrication. Measurements of the copper wire chaff also allowed a comparison with existing theoretical predictions of chaff reflectivity. An analysis and a comparison of the results is presented. Results show that the experimental trends of the chaff RCS curves agree with the theoretical RCS curves for perfectly conducting wires. They also show that copper wire provides the strongest reflective chaff followed by the aluminised glass and the microwire.

**KEYWORDS**

electronic countermeasures, radar cross-sections

## 1 | INTRODUCTION

Chaff has been widely used to passively counter the detection and tracking capabilities of radar systems since War World II. Chaff consists of single highly reflective elements, such as metallic strips or dipoles that are launched in a cloud with the aim to deceive enemy radars and protect a platform by generating a high reflective false target. Since its first appearance in the early 1940s when it was known as Window, multiple studies have been carried out to characterise the scattering properties of chaff and chaff have been widely improved and updated as a very effective Electronic Counter Measure (ECM) against a large number of different threats and platforms.

A theoretical and experimental study of the RF characteristics of half-wavelength and full-wavelength dipoles is presented in ref. [1] and a comprehensive summary of the history of chaff and their electro-magnetic properties is available in ref. [2]. The bistatic cross-section of chaff was investigated in ref. [3]. Simplified scattering approximations based on the Einarsson's equations of the RCS of thin dipoles with relative plots were presented in ref. [4]. A numerical technique for the time domain simulation of the response of a chaff cloud is available in ref. [5]. Recent research has investigated the scattering characteristics of chaff with a different shape. For example, electromagnetic dipole and Koch snowflake chaff were characterised and compared in ref. [6]. Measurements were gathered with an experimental technique based on Inverse Synthetic Aperture Radar (ISAR) to test single chaff elements in an anechoic chamber. To do this, single chaff and small chaff arrays were printed on a fibreglass substrate and placed on a rotating stand to collect multi-perspective signatures for ISAR processing. The aim of this study was to inform further predictions of chaff clouds. Recent work on chaff has investigated new chaff identification methods that integrate the distribution of distance, Doppler frequency, and power in Range-Doppler imaging [7] and a Pre-Decluttering Dual-Stage UNet with a multi-stage loss function to achieve progressive training [8].

Although previous work has mostly focussed on understanding the RCS properties of single chaff elements in order to study and simulate the expected performance of chaff clouds, the reflective characteristics of chaff also provide key information to design and compare different chaff types, different element compositions and different fabrication techniques. The aim of the work presented in this paper is to develop an experimental setup to allow measurements of chaff dipole elements, over a large bandwidth, in free space and with no requirement for an anechoic chamber. The setup is used to collect reflectivity data from chaff made of copper-wire, microwire and aluminised glass and subsequently to compare chaff RCS characteristics with respect to the existing theory, composition material and fabrication process. The results are important as they can inform further developments and analyses of the RCS characteristics of new type of chaff.

## 2 | EXPERIMENTAL SETUP

The measurement setup consists of a LinearX precision turnable, a MS46322A Anritsu Vector Network Analyser (VNA), two identical horn antennas and a PC. A photo of the setup is shown in Figure 1. The turntable is mounted on the vertical face of a L-shaped metallic frame (Figure 1) and its position can be adjusted by screwing in and out a set of bolts so to ensure it is perfectly aligned perpendicularly to the ground floor. The turntable is capable of rotating with an angular resolution of 0.1° and can be fully controlled remotely with a set of pre-defined commands which are sent through a serial cable from the PC. A 50 cm long metallic cylindrical arm is attached to the centre of rotation of the turntable and carries the two identical horn antennas which are used to transmit and receive the signals generated by the VNA. The antennas are arranged so that they transmit and receive in vertical polarisation (VV) at −90° and at +90°, and in horizontal polarisation (HH) at 0°. As a reference, the positive direction of rotation is clockwise. The target under test is placed in the antenna far-field and faces the antennas on a stand made of styrofoam material. The length of the stand is equal to the height of the antennas with respect to the ground floor, so that elements are measured at 0° elevation angle. Rotating the turntable allows measurements of the target response from different polarisation aspect angles.

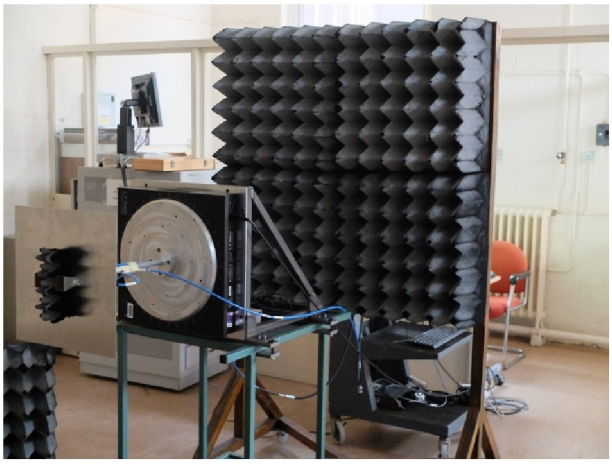

**FIGURE 1** Measurement setup.

The Anritsu VNA used to transmit and receive can operate in the range of frequencies from 40 MHz up to 40 GHz. At each aspect angle, it measures the impulse response of the target over a pre-defined bandwidth $B$. It produces the amplitude and phase of the target frequency response over a maximum of up to 16,001 frequency points $(f_i)$ within the selected bandwidth.

The turntable and the VNA are connected to the PC with a serial cable and an ethernet cable, respectively, and are fully controlled and synchronised with LabView. The Labview scripts were developed so to ensure that the VNA collects the target frequency response at the initial angle before triggering the rotation of the turntable of the step in degrees. The setup then waits for a user-defined waiting time (usually approximately 10 s) to acquire the data from the new aspect angle in order to ensure the setup is completely stationary during each measurement.

Measurements were collected from 5 to 11 GHz, over two frequency bandwidth measurements, and the characteristics of the horn antennas used are given in Table 1. RAM material was positioned around the rig and between the transmitting and receiving antennas to improve isolation and eliminate the effects of different objects in the surrounding open laboratory area. Dipoles were attached to a nylon monofilament approximately 0.25 mm diameter using 3M Spray Mount™ repositionable adhesive. A copper wire, chaff or microwire length is laid on a matt black board and cut with a scalpel to the nominal dipole length measured with a small steel rule. The nylon line is prepared by marking it in 2 places using a marker pen. The marks are separated by a distance equal to 5–10 mm greater than the intended dipole length. This identifies the intended location of the dipole. The line is sprayed with a small amount of the adhesive and applied using the 2 marks for location to the dipole on the black board. The adhesive picks up the dipole. The dipole can then be examined under a low power binocular microscope and measurements of its length using a Vernier calliper. Dipoles on nylon lines were kept in lengths of plastic drinking straws to protect the dipole and to identify it with a sticker applied to the straw. An example is shown in Figure 2.

The nylon line with the dipole attached is then mounted in a U-shaped foam block as shown in Figure 3. The block has slots cut in each side to accept the line and the line is centred in the U by reference to the red marks. Test were also done to check that the U-shaped foam block and an empty nylon line

**TABLE 1** Horn antenna characteristics.

| Frequency [GHz] | Aperture dimensions [cm] |
|---|---|
| 10 | 4 × 3 |
| 6 | 11.5 × 9 |

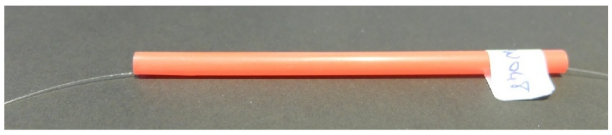

**FIGURE 2** Dipole on a nylon monofilament protected in a length of drinking straw.

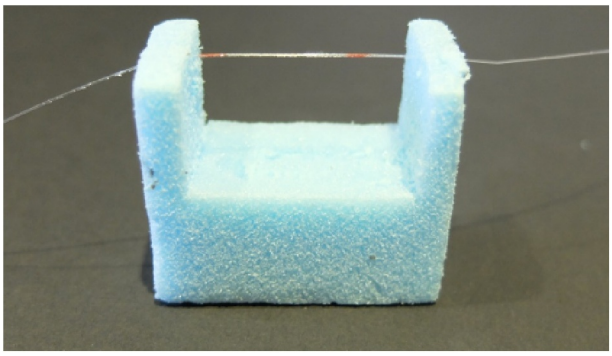

**FIGURE 3** Photo of the filament under test in the stereo-foam support.

without a dipole could not be detected against the RF background. Care is taken when inserting the line and dipole to ensure that is horizontal to within a few degrees.

A measurement of the background was taken and subtracted from each measurement of a chaff element. The VNA data were then converted to the time domain so that range-gating could be applied to isolate the chaff return from any residual background reflections and multipath contributions. This same procedure was repeated for a 3 cm diameter metallic sphere which was used for data calibration.

## 3 | RESULTS

Aluminised glass fibres were taken from standard production material manufactured by Chemring Countermeasures at High Post, Salisbury. These consist of glass fibres with a nominal diameter of 20 $\mu$m coated with aluminium with an average thickness of 1.5 $\mu$m. Therefore, the nominal overall diameter is 23 $\mu$m. Bundles of aluminised glass 50.8 mm long were guillotine cut at Chemring. 50.8 mm dipoles were sampled at random and cut to appropriate shorter lengths for RF measurement as described earlier. Copper microwire fibres consists of a glass fibre with a nominal diameter of 14 $\mu$m with a concentric copper core 8 $\mu$m in diameter. Microwire is produced by the Taylor wire process using a machine that collects a continuous fibre many kilometres long on a plastic spool. Microwire samples were taken at random from several spools. A reel of 100 $\mu$m diameter copper wire was obtained and used to cut the copper wire dipoles. The copper wire was used as a reference material being a pure material without being associated with a glass substrate or a glass outer coating. Figure 4 shows the RCS as a function of frequency for the five longest copper wire dipoles in the band from 5 to 8 GHz. Similarly,

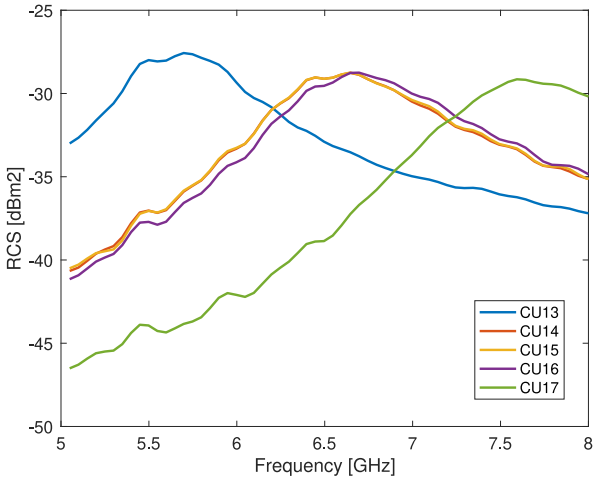


**FIGURE 4** RCS of the copper wire dipoles as a function of frequency in the bandwidth between 5 and 8 GHz.

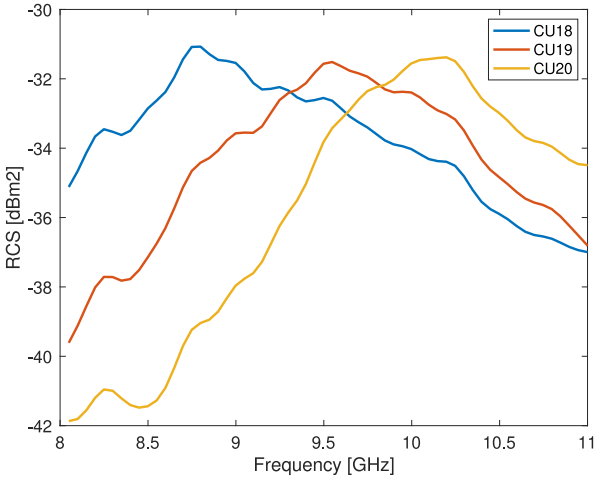


**FIGURE 5** RCS of the copper wire dipoles as a function of frequency in the bandwidth between 8 and 11 GHz.

Figure 5 shows the RCS curves for the shortest dipoles. In both figures, results show a reduction of the peak RCS as an inverse function of the dipole length and a shift of the RCS peaks to higher frequencies as the dipole length is reduced. This result is in agreement with the existing literature [1, 2]. Figure 6 shows the measured calibrated peak RCS of all the copper wire dipoles versus the measured resonant frequency at which each peak occurs. These results are also compared with the expected theoretical curves (dashed line) for a half-wavelength dipole [1] (i.e. a dipole which is assumed to resonate at $\lambda = L/2$, where $L$ is the dipole length) for which the peak RCS $\sigma_{\max}$ can be expressed as follows:

$$\sigma_{\max} = 0.86\lambda^2 \tag{1}$$

The length of all the measured dipoles as the values of the peak RCS and corresponding resonant frequencies are given in Table 2.

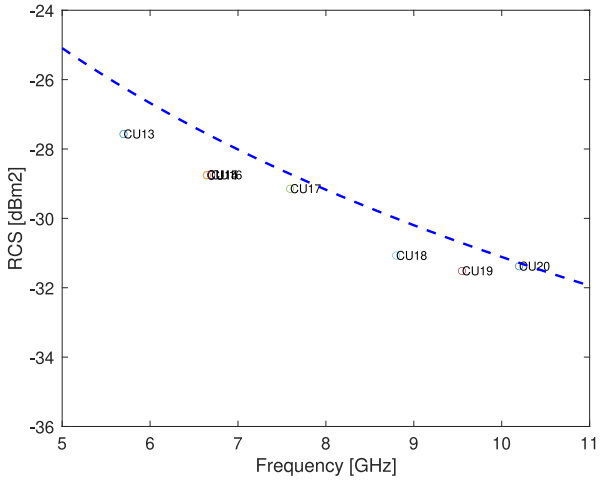


**FIGURE 6** Peak RCS for each copper wire dipole as a function of the frequency at which the peak occurs. The blue dashed curve indicates the expected theoretical RCS as a function of frequency.

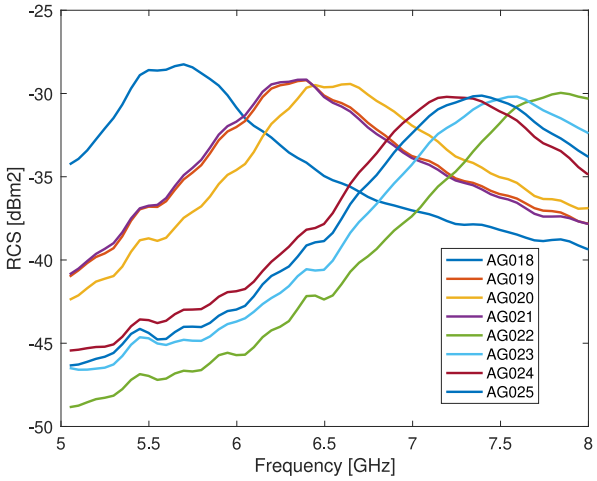


**FIGURE 7** RCS of the aluminised glass dipoles as a function of frequency in the bandwidth between 5 and 8 GHz.

**TABLE 2** Copper dipole Lengths with their theoretical versus measured RCS and resonant frequency.

| | | Peak frequency [GHz] | | Peak RCS [dBm] | |
|---|---|---|---|---|---|
| | Length [mm] | (T) | (M) | (T) | (M) |
| Cu13 | 22.92 | 6.23 | 5.69 | −27 | −27.57 |
| Cu14 | 20.00 | 7.14 | 6.64 | −28.19 | −28.75 |
| Cu15 | 20.28 | 7.04 | 6.64 | −28.07 | −28.74 |
| Cu16 | 19.70 | 7.25 | 6.69 | −28.32 | −28.75 |
| Cu17 | 17.11 | 8.34 | 7.59 | −29.54 | −29.15 |
| Cu18 | 14.66 | 9.74 | 8.80 | −30.88 | −31.07 |
| Cu19 | 13.96 | 10.15 | 9.55 | −31.24 | −31.52 |
| Cu20 | 13.14 | 10.77 | 10.20 | −31.76 | −31.38 |

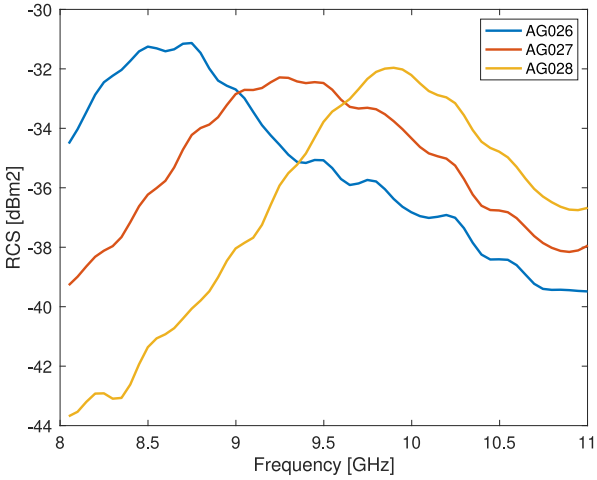


**FIGURE 8** RCS of the aluminised glass dipoles as a function of frequency in the bandwidth between 8 and 11 GHz.

The same results are presented in Figures 7–9 for the aluminised Glass and in Figures 10–12 for the microwire. Similarly, Tables 3 and 4 give the length and the values of the peak RCS and corresponding resonant frequencies for all the aluminised glass and microwire dipoles. The behaviour of the results remains consistent with what was observed for the copper wire dipoles, with a positive shift of resonant frequency as an inverse function of the dipole length and a reduction of the maximum RCS as the resonant frequency increases. The comparison with the half-wavelength dipole theoretical curves show that shape and trend of the experimental curves are consistent with the theory but with an offset that indicates a reduction of the overall RCS as the dipole material changes. This can be seen clearly in Figure 13 where a direct comparison between the three materials is presented. Results indicate that, on average, the copper provides higher reflectivity followed by the aluminised glass and the microwire, with the latter being the weakest reflector.

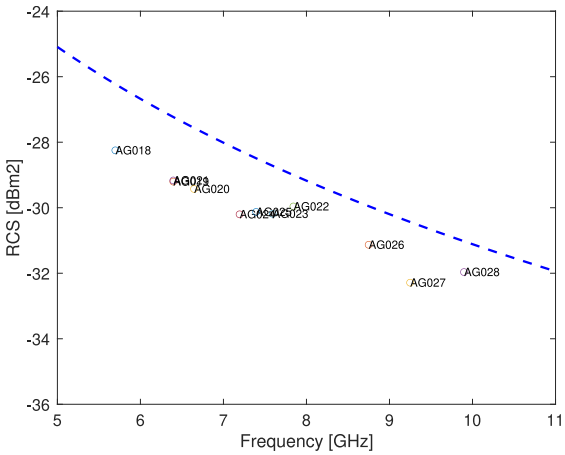


**FIGURE 9** Peak RCS for each aluminised glass dipole as a function of the frequency at which the peak occurs.

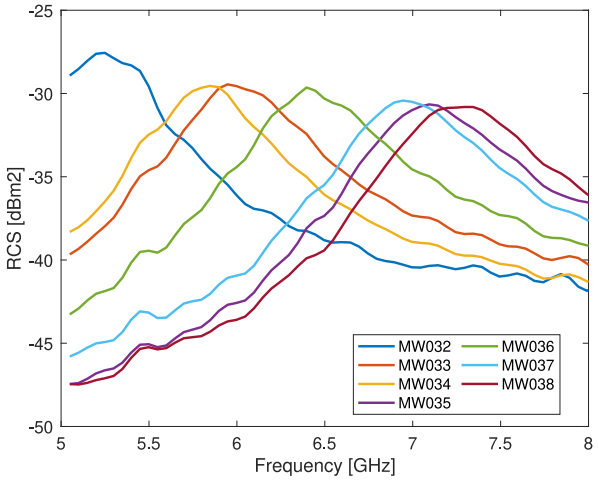


**FIGURE 10** RCS of the microwire dipoles as a function of frequency in the bandwidth between 5 and 8 GHz.

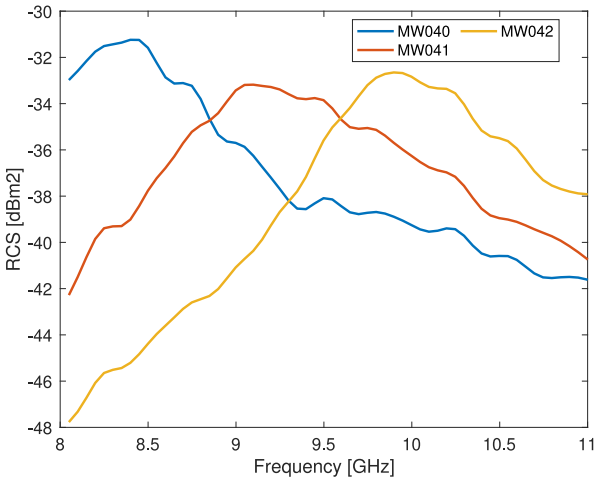


**FIGURE 11** RCS of the microwire dipoles as a function of frequency in the bandwidth between 5 and 8 GHz.

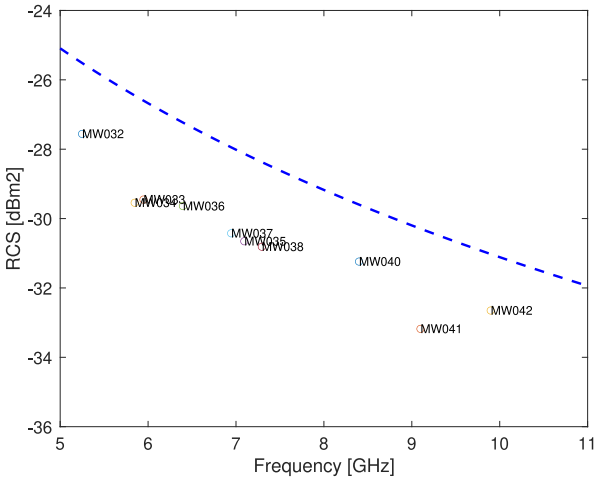


**FIGURE 12** Peak RCS for each microwire dipole as a function of the frequency at which the peak occurs.

**TABLE 3** Aluminised Glass dipole lengths with their theoretical (T) versus measured (M) RCS and resonant frequency.

| | Length [mm] | Peak frequency [GHz] | | Peak RCS [dBm2] | |
|---|---|---|---|---|---|
| | | (T) | (M) | (T) | (M) |
| AG018 | 23.51 | 6.15 | 5.70 | −26.89 | −28.25 |
| AG019 | 20.29 | 7.13 | 6.40 | −28.17 | −29.20 |
| AG020 | 20.27 | 7.13 | 6.65 | −28.18 | −29.43 |
| AG021 | 20.34 | 7.11 | 6.40 | −28.15 | −29.17 |
| AG022 | 16.69 | 8.63 | 7.84 | −29.83 | −29.96 |
| AG023 | 17.36 | 8.29 | 7.59 | −29.49 | −30.19 |
| AG024 | 18.17 | 7.96 | 7.19 | −29.13 | −30.20 |
| AG025 | 17.39 | 8.28 | 7.39 | −29.47 | −30.13 |
| AG026 | 14.65 | 9.83 | 8.75 | −30.96 | −31.13 |
| AG027 | 13.93 | 10.34 | 9.25 | −31.40 | −32.29 |
| AG028 | 12.89 | 11.17 | 9.90 | −32.08 | −31.96 |

**TABLE 4** Microwire dipole lengths with their theoretical (T) versus measured (M) RCS and resonant frequency.

| | Length [mm] | Peak frequency [GHz] | | Peak RCS [dBm2] | |
|---|---|---|---|---|---|
| | | (T) | (M) | (T) | (M) |
| MW032 | 22.65 | 6.41 | 5.25 | −27.25 | −27.56 |
| MW033 | 19.55 | 7.43 | 5.95 | −28.53 | −29.45 |
| MW034 | 19.89 | 7.30 | 5.85 | −28.38 | −29.54 |
| MW035 | 19.56 | 7.42 | 7.09 | −28.53 | −30.65 |
| MW036 | 18.34 | 7.92 | 6.40 | −29.08 | −29.64 |
| MW037 | 17.23 | 8.43 | 6.94 | −29.63 | −30.43 |
| MW038 | 16.49 | 8.81 | 7.29 | −30.01 | −30.81 |
| MW040 | 13.82 | 10.51 | 8.40 | −31.54 | −31.24 |
| MW041 | 12.36 | 11.74 | 9.10 | −32.51 | −33.18 |
| MW042 | 11.69 | 12.42 | 9.90 | −33.00 | −32.65 |

## 3.1 | Accuracy analysis

Previous measurements have shown that the accuracy of the setup presented in this paper falls within ±2 dB. To measure the extent of errors, chaff measurements are normally assessed by additional measurements of at least two independent spheres of different diameters. Whilst one of the two sphere is used for calibration, the measured RCS of the second sphere is used to analyse errors with respect to its expected theoretical RCS. Figure 14, for example, shows the measured calibrated RCS of a 30 mm diameter metallic sphere from 8 to 11 GHz, obtained by using a 38 mm metallic sphere for calibration.

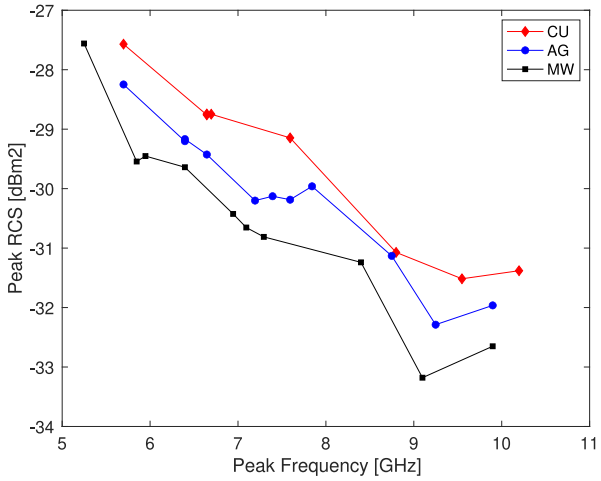


**FIGURE 13** Comparisons of dipole RCS values.

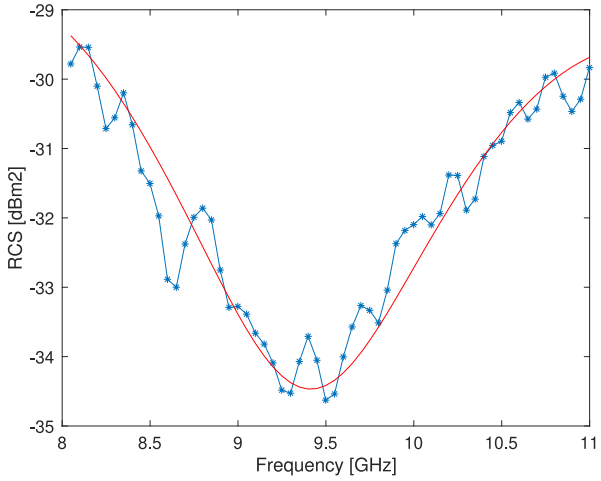


**FIGURE 14** Measured RCS (blue) of a 30 mm diameter sphere versus expected theoretical curve (red). Results are obtained after calibration with a 38 mm calibration sphere.

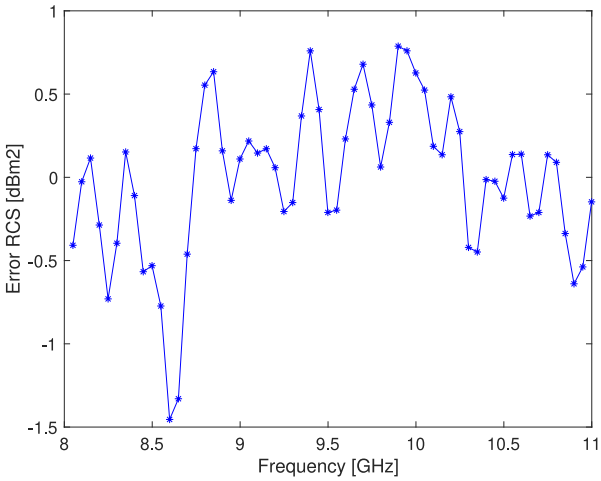


**FIGURE 15** RCS error for the measured RCS of a 30 mm diameter sphere. Results are obtained after calibration with a 38 mm calibration sphere.

Figure 15 shows the difference between the two curves in Figure 14 indicating that errors are contained within the ±2 dB range. Sources of error include Signal to Noise Ratio (SNR), unresolved undesired interactions between the target (or the antennas) with the surrounding equipment (i.e. the styrofoam stand) as well as imperfections of the calibrating targets. Averaging multiple measurements further improves the measurement accuracy at the expense of longer collection times.

## 4 | DISCUSSION

The measurement method is intended to evaluate the radar cross section of aluminised glass, the most common chaff material, and to compare it with a reference material and other potential chaff materials. Microwire is used as an example. Other materials have been evaluated but the results are not reported here.

It should be borne in mind that the performance of a chaff payload in the real world depends on many factors [2]. These include the dipole diameter, the dipole length, the surface properties and the dispensing method. In a dense chaff cloud, multiple scattering will occur. The RCS of a single chaff dipole in a chaff cloud is only fully realised when the dipoles are separated by $2\lambda$ or more, where $\lambda$ is the radar wavelength.

Clumping or birdnesting occurs with all chaff materials where, on dispensing, many dipoles are locked together and never act as free dipoles with their expected RCS. With its very smooth glass surface, microwire would appear to be a material that disperses very well. However, the glass surface absorbs water from the air and adjacent fibres are strongly bound to each other by hydroxyl bonds. To minimise birdnesting, slip coats of various types are used depending on the chaff material. A fatty acid is used for aluminised glass [9]. Birdnesting is reduced for larger dipole diameters and shorter dipoles.

For the self-protection of an aircraft, chaff needs to very rapidly produce an RCS larger than the aircraft RCS within the radar resolution cell to break the radar lock. From simple calculations of aircraft velocities and the radar characteristics, the larger RCS must be achieved typically within 0.5s. Within this time, little if any of the dipoles are separated by $2\lambda$. Instead, the chaff cloud acts as a broadband reflector where the RCS is equal to the area of the chaff cloud [10].

Current aircraft dispensers are of two broad types; pyrotechnic and electromechanical. A pyrotechnic dispenser such as the ALE-47 typically employs broadband chaff cartridges that include several packages of different dipole lengths. These will eject about 50% of the dipoles in the form of clumps or birdnests. An electromechanical dispenser, such as BOL, releases a rapid sequence of smaller broadband packages directly into an airstream. BOL is usually mounted in a missile launcher. Chaff dispersal is enhanced by the turbulent airstream behind the missile launcher rail and by vortex generators fitted to the dispenser head. BOL achieves lower birdnesting and better overall dispersion than pyrotechnic cartridges. Further advantage can be gained by dispensing simultaneously from dispensers on both wings where, from

some aspects, the RCS achieved by each dispenser is additive within the radar resolution cell.

Chaff is highly susceptible to discrimination from the aircraft by Moving Target Indication (MTI) and pulse Doppler radars because, once dispensed, it slows to its terminal velocity (typically 0.3 m/s) very rapidly. This can be counteracted to some extent by dispensing with manoeuvre so that the aircraft presents zero or near zero velocity return to such radars.

## 5 | CONCLUSIONS

A free space test method was presented and used to measure the Radar Cross Section (RCS) of single dipole elements made of copper wire, microwire and aluminised glass. Measurements were taken from 5 to 11 GHz to allow a comparison of chaff RCS properties with respect to chaff material and methods of fabrication. Measurements of the copper wire chaff also allowed comparisons with available theoretical predictions of chaff reflectivity. The experimental results have shown that the behaviour of the chaff RCS agrees with the theoretical RCS curves for perfectly conducting wires. Copper wire provided the strongest reflective chaff followed by the aluminised glass and the microwire.

The method allows comparison of candidate chaff materials, but the ultimate performance of chaff relies on many other aspects of its material properties, the dispensing method and the radar system that it is intended to counter.

## AUTHOR CONTRIBUTIONS

**Alessio Balleri**: Data curation; formal analysis; investigation; methodology; software; validation; visualization; writing—original draft. **Brian Butters**: Conceptualization; data curation; funding acquisition; investigation; methodology; project administration; resources; supervision; validation; visualization; writing—review & editing.

## ACKNOWLEDGEMENTS

This work has been supported by the UK MOD Centre for Defence and Enterprise (CDE 33811 Phase 2 –Research and Development into Chaff Improvement Programme Phase 2). Dstl Contract No. DSTL/AGR/00623/01. For the purposes of open access, the author has applied a Creative Commons Attribution (CC BY) licence to any Accepted Author Manuscript version arising from this submission.

## CONFLICT OF INTEREST STATEMENT

This is to confirm there is no conflict of interest associated with this research and this publication.

## DATA AVAILABILITY STATEMENT

Data supporting this study cannot be made available due to commercial restrictions.

## ORCID

*Alessio Balleri* https://orcid.org/0000-0001-6185-1165

## REFERENCES

1. Mack, C.L., Reiffen, B.: Rf characteristics of thin dipoles. Proc. IEEE 52(5), 533–542 (1964). https://doi.org/10.1109/proc.1964.2994
2. Butters, B.C.F.: Chaff. In: Communications, Radar and Signal Processing, IEE Proceedings F, pp. 197–201 (1982). https://doi.org/10.1049/ip-f-1.1982.0030
3. Peebles, P.Z.: Bistatic radar cross sections of chaff. IEEE Trans. Aero. Electron. Syst. 20(2), 128–140 (1984). https://doi.org/10.1109/taes.1984.310435
4. Nagl, A., Ashrafi, D., Uberall, H.: Radar cross section of thin wires. IEEE Trans. Antenn. Propag. 39(1), 105–108 (1991). https://doi.org/10.1109/8.64443
5. Winchester, T.A.: "A time domain characterisation of the pulsed radar return from a chaff cloud," DSTO Australia, Electronic Warfare Division. Tech. Rep. (1992). http://www.dtic.mil/dtic/tr/fulltext/u2/a257424.pdf
6. Scholfield, D., et al.: A new technique for the characterization of chaff elements. Rev. Sci. Instrum. 82(7) (2011). https://doi.org/10.1063/1.3606449
7. Wang, H., et al.: Chaff identification method based on range-Doppler imaging feature. IET Radar, Sonar Navig. 16(11), 1861–1871 (2022). https://doi.org/10.1049/rsn2.12302
8. Xu, Q., et al.: Chaff jamming recognition and suppression based on semi-realistic dataset and pre-decluttering dual-stage unet. IET Radar, Sonar Navig. 18(8), 1291–1306 (2024). https://ietresearch.onlinelibrary.wiley.com/doi/abs/10.1049/rsn2.12569
9. Butters, B.F.C., Pollicott, I.D.: Slip coating chaff. U.S. Patent 4(649 076) (1987)
10. Kownacki, S.: Screening (shielding) effect of a chaff cloud. IEEE Trans. Aero. Electron. Syst. AES-3(4), 731–734 (1967). https://doi.org/10.1109/taes.1967.5408853

**How to cite this article:** Balleri, A., Butters, B.: Measurements and analysis of the radar cross section of chaff dipoles. IET Radar Sonar Navig. 1–7 (2024). https://doi.org/10.1049/rsn2.12654

# Measurements and analysis of the radar cross section of chaff dipoles

Balleri, Alessio

2024-11



Balleri A, Butters B. (2024) Measurements and analysis of the radar cross section of chaff dipoles. IET Radar, Sonar & Navigation, Volume 18, Issue 11, November 2024, pp. 2182-2188
https://doi.org/10.1049/rsn2.12654